

Ionosphere Threat Space Model

Assessment for GBAS

C. Mayer, B. Belabbas, N. Jakowski, M. Meurer, *German Aerospace Center*

W. Dunkel, *DFS Germany*

ABSTRACT

Ground Based Augmentation Systems (GBAS) can correct the majority of the GNSS pseudo range errors experienced by an aircraft in the vicinity of an airport. The "normal" behavior of the ionosphere has a very limited impact on the position error; the confidence interval of the user position is fully acceptable for precision approach. Unfortunately, the ionosphere medium is sometimes subject to perturbations due to the strong temporal and spatial variability of the ionospheric plasma.

While most of the time this environmental effect is behaving in a normal way, there has been found an anomalous ionospheric behavior which occurs rarely (few occurrences in 10 years) in mid latitudes but can be a serious threat to GBAS integrity. The CAT I GBAS architecture can principally not fully mitigate these effects by monitoring.

In order to use the proposed mitigation algorithms for the ionosphere threat in a different geographical region, the anomalous ionosphere threat model has to be established for the relevant region. For the certification of a GBAS ground facility in Germany, both the anomalous ionosphere threat space and the nominal ionospheric decorrelation for a region including Germany were determined.

This work has been done within the ITMA (ionosphere threat model assessment) project which is a joint project between the German Air Navigation Service Provider DFS and the German Aerospace Center DLR, funded by DFS.

INTRODUCTION

Not corrected (spatially uncorrelated) errors between ground and airborne subsystems must be over-bounded and kept as small as possible in order to reach the required level of integrity defined by ICAO.

Ionosphere gradients remain in general very small, e.g. they can be bounded by 4 mm/km in the CONUS

(conterminous US) region. When GNSS signals received by the aircraft are delayed in a different way than the GNSS signals received by the GBAS ground facility (GGF), the corrections provided by the GGF can cause unacceptably large position errors at aircraft level.

The CAT I GBAS architecture can principally not fully mitigate these effects by monitoring. According to the agreed approach in the GBAS CAT I community, the remaining risk is therefore treated as follows: At each epoch the worst-case ionospheric threat is assumed to occur in 100% of the time. The threat is mitigated, e.g., by preventing the aircraft from using unsafe combinations of GNSS satellites [4], [5].

To permit the analysis, it is essential to first define the ionosphere threat space. Since the anomalous ionosphere threat consists of moving ionospheric fronts, the ionosphere threat space is spanned by the slope, velocity and width of such an ionospheric front, cf. Fig 1.

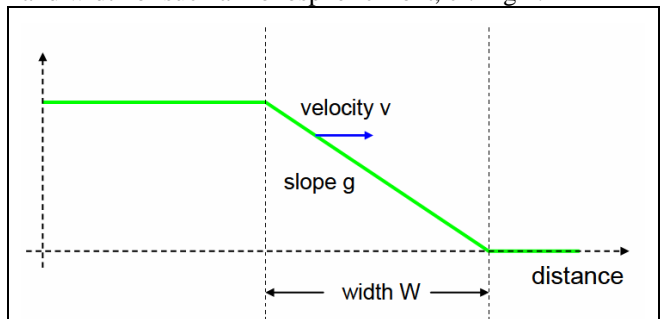


Fig 1: GBAS Anomalous Ionosphere Threat Model

DATA SCREENING

In order to find periods with a disturbed ionosphere, we have performed an extensive data screening using publicly available data from the 11-year period between 1998 and 2008. The data basis is shown in Fig 2. For the data screening we have used all available data in the geographic region $2^{\circ}\text{E} - 18^{\circ}\text{E}$, $45^{\circ}\text{N} - 58^{\circ}\text{N}$ which includes Germany.

Instead of relying solely on geo-magnetic indices, we have analyzed GPS data using $grad_{ROT}$ as test variable [1], [2] which is defined as

$$grad_{ROT} = \frac{I_{phase_diff}(t_1) - I_{phase_diff}(t_2)}{\Delta s},$$

where I_{phase_diff} are the relative ionospheric delays computed from the difference of phase measurements on L1 and L2 of two consecutive epochs t_1 and t_2 ; Δs is the distance of the corresponding ionosphere pierce points, using the thin-shell approximation of the ionosphere with height 350 km. Thus, $grad_{ROT}$ are spatial gradients computed from the rate of change (ROT – rate-of-TEC).

Since $grad_{ROT}$ contains a mix of spatial and temporal gradients, we have developed methods for estimating the velocity of ionospheric disturbances in order to correct $grad_{ROT}$ for the motion of ionosphere. Nevertheless, $grad_{ROT}$ can be used as an indicator for detecting ionospheric disturbances.

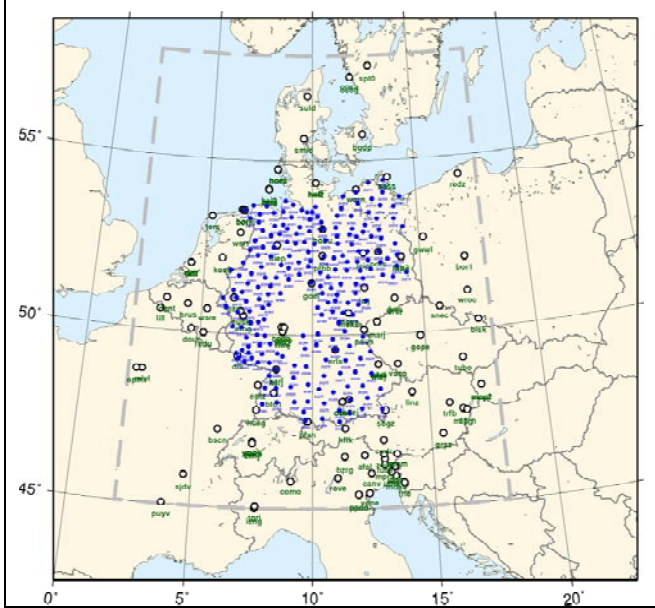


Fig 2: Data basis used in the ITMA study: green – ground stations (IGS,EUREF,GREF) used in data-screening, blue – ground stations (SAPOS) used in threat model analysis.

We have computed $grad_{ROT}$ for all available data between 1998 and 2008, and then selected those days where $grad_{ROT}$ exceeds certain thresholds. Since we use phase observables, a simple heuristic filtering is applied which removes, e.g., cycle slips and other bad data. Each event found by the data screening was checked manually,

also using code-minus-carrier (CMC) and code-difference observables.

Fig 3 shows the result of data screening for the year 2003. The well-known storms from October and November 2003 are clearly seen as enhanced $grad_{ROT}$ -values. However the November 20 storm, which has produced the most extreme gradients in the CONUS region, shows a relatively small number of data points exceeding $grad_{ROT} = 100$ ppm already indicating that this storm was less severe in the area under consideration. For each selected day, the locations of the biggest gradients have been plotted in order to narrow the scope of the threat model analysis, cf. Fig 4.

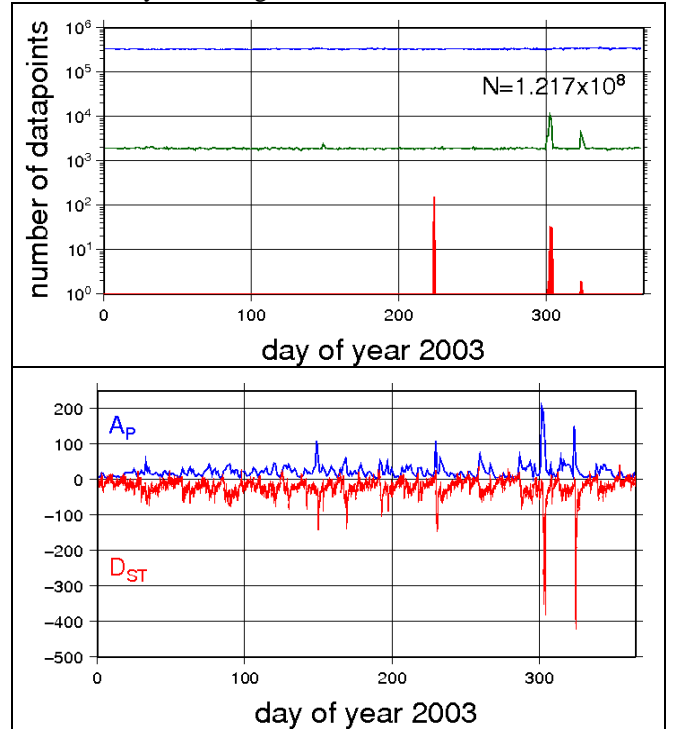


Fig 3: Top plot: blue – total number of data points per day, green – number of bad data points per day, red – number of data points with $grad_{ROT} > 100$ ppm. Bottom plot: A_P and D_{ST} Indices for 2003.

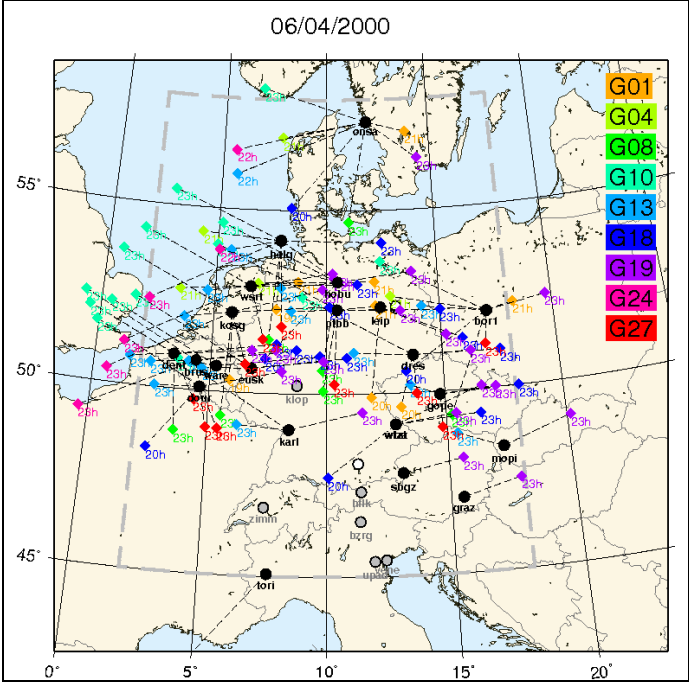


Fig 4: The locations (ionosphere pierce points) of the maximal gradients for each pair of ground station and GPS satellite exceeding 50 mm/km are shown as diamonds. The black circles indicate the locations of ground stations used for the data screening.

NOMINAL IONOSPHERIC GRADIENTS

In order to determine *nominal* vertical gradients, we have selected the periods of quiet geo-magnetic conditions shown in Tab 1.

	High Solar Activity (HSA)	Low Solar Activity (LSA)
Winter	2001-001 – 2001-010	2007-154 – 2007-159
Summer	2001-149 – 2001-158	2007-356 – 2007-363

Tab 1: Data used for determination of σ_{VIG} .

For these periods we have computed calibrated vertical TEC, cf. [6]. Vertical ionosphere gradients are formed by dividing the difference between IPPs at the same epoch by the distance between the IPPs. The number of used data points is shown in Tab 2.

Period	Number of data points
HSA Winter	114903
HSA Summer	91630
LSA Winter	322675
LSA Summer	241245
$\Sigma = 810273$	

Tab 2: Number of data points used for estimating σ_{VIG} .

The σ_{VIG} -overbound for the region “Germany” is found to be 2.07 mm/km, cf. Fig 5.

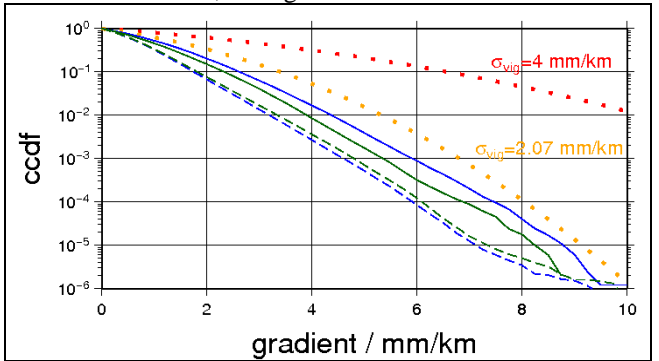


Fig 5: Shown are CCDFs for vertical ionosphere gradients. Blue – winter, green – summer, solid line – HSA, dashed line – LSA, dotted lines – Gaussian overbounds.

THREAT MODEL PARAMETER ESTIMATION

Around each disturbance we use a local coordinate system which is defined by

$$\begin{pmatrix} x_1 \\ x_2 \end{pmatrix} = 117.6 \text{ km} \cdot \begin{pmatrix} \cos(\text{lat}_0) & 0 \\ 0 & 1 \end{pmatrix} \cdot \begin{pmatrix} \text{lon} \\ \text{lat} \end{pmatrix}.$$

These coordinates are valid in a small region around a given reference location $(\text{lat}_0, \text{lon}_0)$ only, and refer to distances at the height of the thin-shell approximation of the ionosphere.

When determining the velocity of a front, the spatial evolution of the front has to be tracked. Therefore, the occurrence of the font at each ground stations has to be determined. Since there are many ways of defining front occurrence, e.g. using the steepest gradient, or the beginning/end of the disturbance, we use the cross-correlation between a reference signal and the signals of other stations

$$cc(x, y) = \frac{\langle x \cdot y \rangle}{\sqrt{\langle x^2 \rangle \langle y^2 \rangle}}.$$

The maximal cross correlation determines a time offset Δt , which we use to fix the occurrence of a disturbance relative to the references signal. In Fig 6 an example of two $grad_{ROT}$ -signals together with the cross-correlation is shown.

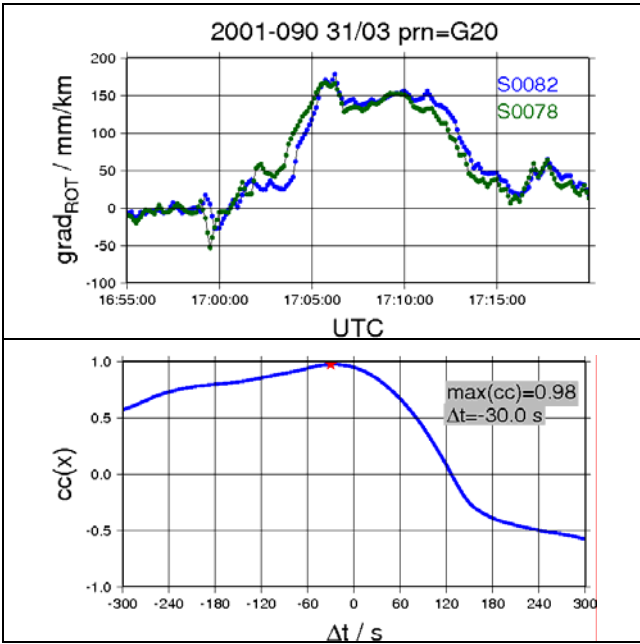


Fig 6: Cross-correlation technique for finding the time offset between two signals. Top: grad_{ROT} of two stations bottom: cross-correlation for different time offsets Δt .

After pre-processing we obtain a collection $\{\vec{x}_i, t_i\}_{i=1}^N$ of front locations \vec{x}_i and corresponding times t_i . This is the basis for determining the velocity of the front.

Velocity

We assume that the disturbance can be described by an ideal plane wave:

$$\vec{x}(t, \lambda) = \vec{x}_0 + t \cdot \vec{v} + \lambda \cdot \vec{u}$$

Here, \vec{x}_0 is a base point, \vec{v} is the velocity and the vector \vec{u} is perpendicular to \vec{v} . Thus, the parameter t governs the linear propagation of the wave front, while the parameter λ parameterizes the wave-front itself, cf. Fig 7.

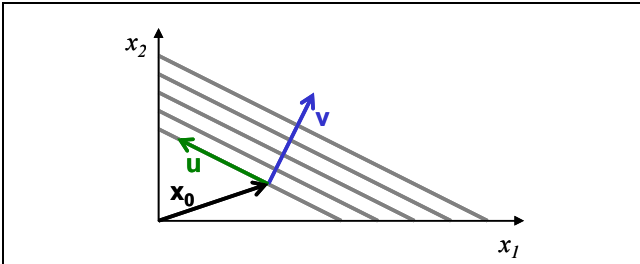


Fig 7: Ideal model of a linear front with velocity \vec{v} . The vector \vec{u} is perpendicular to \vec{v} .

In the following we use the data shown in Fig 8 in order to demonstrate two independent ways of determining the velocity of a front.

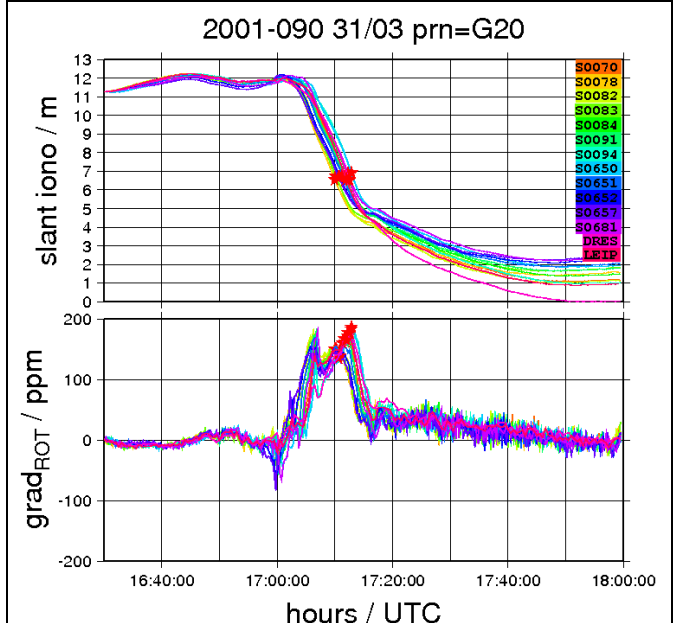


Fig 8: Top: The relative slant iono delays show a front-like shape. The bottom plot shows the corresponding grad_{ROT} -values and the front occurrences as red stars. Note that the gradients grad_{ROT} are not corrected for the movement of the front.

Method (I): Least-squares

When we insert the position and times $\{\vec{x}_i, t_i\}_{i=1}^N$ of front occurrence into the model of an ideal front,

$$\vec{x}_i = \vec{x}_0 + t_i \cdot \vec{v} + \lambda_i \cdot \vec{u},$$

multiply this equation with \vec{v} and divide by v^2 , we obtain the following linear system of equations:

$$\begin{pmatrix} \vec{x}_1^T & -1 \\ \vec{x}_2^T & -1 \\ \vdots & \vdots \\ \vec{x}_N^T & -1 \end{pmatrix} \begin{pmatrix} \vec{k} \\ a \end{pmatrix} = \begin{pmatrix} t_1 \\ t_2 \\ \vdots \\ t_N \end{pmatrix} \quad a \equiv (\vec{x}_0 \bullet \vec{u}) \quad \vec{k} \equiv \vec{v}/(\vec{v} \bullet \vec{v})$$

For $N = 3$ this system of equation is solvable, when $N > 3$ is can be solved using the least-squares method. The velocity vector \vec{v} is inverse to the vector \vec{k} , i.e.,

$$\vec{v} = \vec{k}/(\vec{k} \bullet \vec{k}),$$

and the azimuth of the front direction is given by

$$\text{azim}(v) = 90^\circ - \text{atan}2(v_2, v_1) \cdot 180^\circ / \pi.$$

With these equations we obtain the front parameters shown in Fig 9.

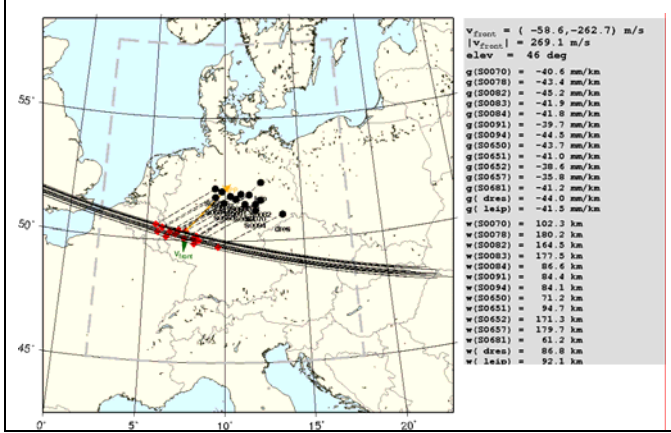


Fig 9: Front parameters for the data example. Note that the extension of the front may be smaller than shown in the plot.

Method (II): Search in parameter space

When we project the front occurrences $\{\vec{x}_i, t_i\}_{i=1}^N$ to a direction determined by an angle α ,

$$x_i(\alpha) = \cos(\alpha) \cdot x_{1,i} + \sin(\alpha) \cdot x_{2,i},$$

we obtain for each angle α a time-distance diagram from which $v(\alpha)$, the velocity projected to α , can be determined by linear regression. Which is the right angle α ? In order to answer this question let us consider the sum of the squares of the fit residuals $\varepsilon_i(\alpha)$:

$$\chi^2(\alpha) = \sum_{i=1}^N \varepsilon_i(\alpha)^2.$$

It can be seen that for an ideal front, $\chi^2(\alpha)$ has a minimum when the angle α corresponds to the azimuth of the front velocity ($\pm 180^\circ$). For the data example the resulting $\chi^2(\alpha)$ and $v(\alpha)$ are shown in Fig 10.

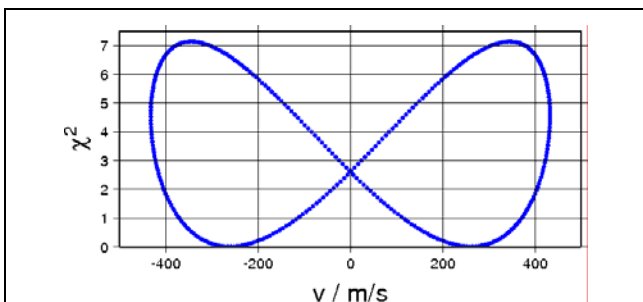


Fig 10: Search in parameter space. The velocity is determined by the minima in χ^2 .

The velocity determined by search in parameter space is $v = \pm 259$ m/s, and the corresponding front directions are $\alpha' = (77^\circ, 257^\circ)$ i.e. $\text{azim}(v) = (13^\circ, 193^\circ)$.

For the data example the results of the two methods are compared in Tab 3:

- The least-squares method (method I) provides absolute value and direction of the front velocity
- The search in parameter space (method II) provides the absolute value of the front velocity and the front direction up to $\pm 180^\circ$.
- The analysed data suggests that method (II) is more robust than method (I)

	Method (I)	Method (II)
$ \vec{v} $	269.14 m/s	± 259 m/s
$\text{azim}(v)$	192.6 $^\circ$	193 $^\circ$, 13 $^\circ$

Tab 3: Comparison of method (I) and (II) for determining the velocity of an ionosphere front.

For each analysed front, we have used both methods for computing the velocity, thus performing a double-check on the results.

The formal error for the determined front velocity is computed using two ways:

- „B-Value“-method: Compute the front velocity $\{v_i\}_{i=1}^N$ from all measurements except the i -th measurement. Then the interval $[\min(v_i), \max(v_i)]$ indicates how good the velocity is determined.
- Another way of estimating the error in the front velocity is to compare the velocities determined by method (I) and method (II).

We use the maximum error of both methods as error in front velocity.

Slope

When the front velocity is known, the slope of the front is determined by the following simple geometrical relationship:

$$g = \frac{dI/dt}{\Delta v}, \quad \Delta v = (\vec{v}_{IPP} - \vec{v}_{front}) \bullet \frac{\vec{v}_{IPP}}{\|\vec{v}_{IPP}\|}.$$

The error for slopes given below is computed as the maximum deviation of the individual slopes from the slope of the front:

$$\Delta g_{front} = \max(|g_{front} - g_i|),$$

where g_i are the slopes corresponding to the velocities v_i .

Width

By an argument similar to the determination of the slope of the front, its width is given by

$$W = \Delta v \cdot T_W,$$

where T_W is the duration of the front in seconds. As a definition of the duration T_W of the front we use the time interval when $|grad_{ROT}|$ is above 80% of its maximal value.

The formal error of the front width is computed similarly to the error in front slopes:

$$\Delta W_{front} = \max(|abs(W_{front} - W_i)|),$$

where W_i are the widths corresponding to the velocities v_i .

RESULTS

We have found 26 ionosphere fronts in the data and analyzed each event w.r.t to all three threat model parameters: velocity, slope and width. In Fig 11 and in Fig 12 the slopes of these events are shown w.r.t. velocity and elevation. A possible domain in the parameter space which contains all events is indicated in red.

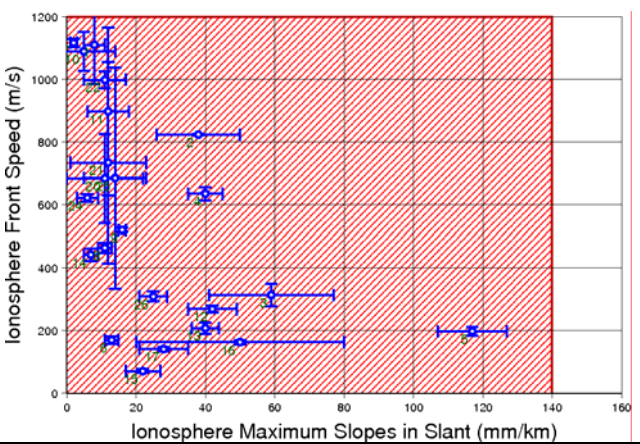


Fig 11: Proposed threat model for the region “Germany”. The analyzed fronts are plotted w.r.t speed and slope.

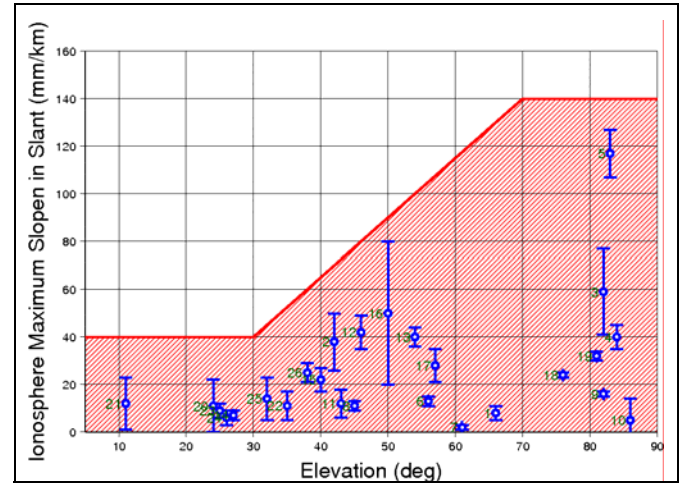


Fig 12: Proposed threat model for the region “Germany”. The analyzed fronts are plotted w.r.t slope and elevation.

The maximal front slope depending on elevation can be parameterized as follows:

$$g_{\max}(elev) = \begin{cases} 40 & , 5^\circ < elev \leq 30^\circ \\ 40 + 2.5 \cdot (elev - 30) & , 30^\circ < elev \leq 70^\circ \\ 140 & , 70^\circ < elev \leq 90^\circ \end{cases}$$

Since the event with maximal slope has been determined using data from three stations only, we have made a time-distance diagram for this event using the data of more than 20 stations where we have used the positions projected to the front direction as “distance”. The front velocity of about 200 m/s can be seen also in this much larger data sample, which confirms the front velocity found with only three stations.

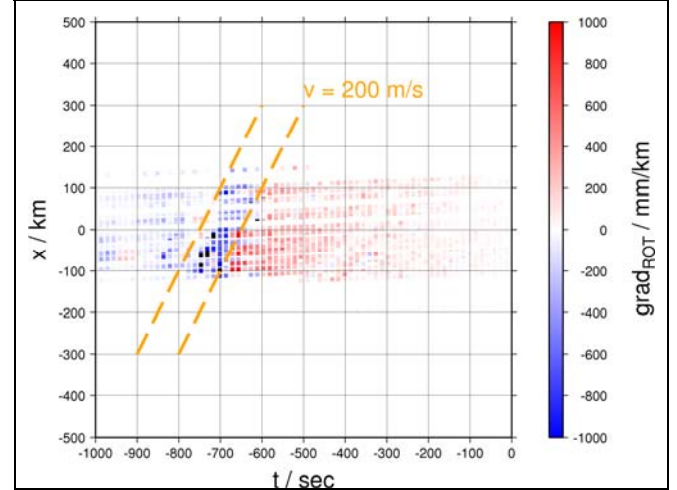


Fig 13: Time-distance diagram for the event with maximal slope. Shown are color-coded $grad_{ROT}$ -values of more than 20 stations. The relative “distance” x is computed from IPP positions projected onto the front direction.

In Fig 14 and Fig 15 the front events found over Germany are plotted along with the parameter domain found in CONUS. The maximal front slopes lie clearly inside the CONUS parameter domain. However there are events with slopes < 50 mm/km which have velocities exceeding the CONUS maximal velocity of 800 m/s.

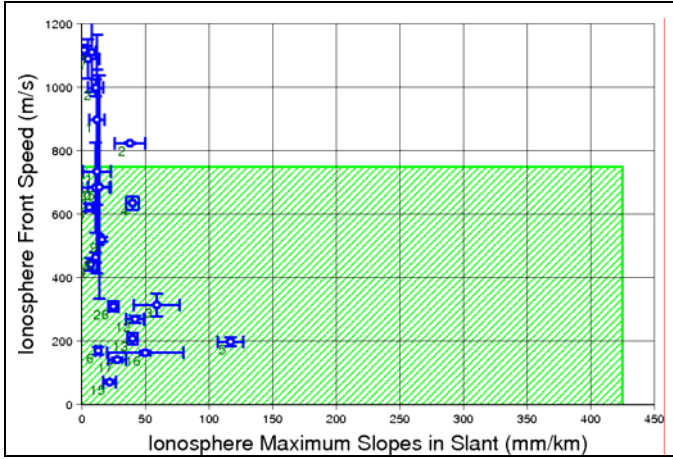


Fig 14: Comparison of the proposed threat model for the region “Germany” with the CONUS threat model.

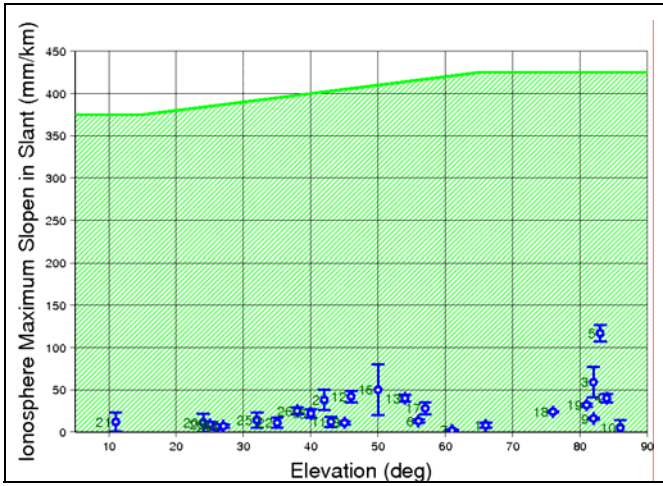


Fig 15: Comparison of the proposed threat model for the region “Germany” with the CONUS threat model.

The most extreme high-velocity event is shown in Fig 16. It has been detected using two different sets of ground stations.

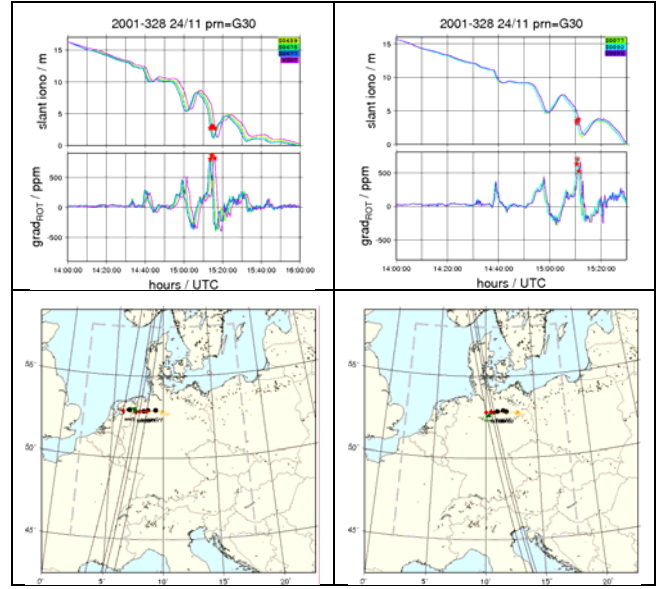


Fig 16: High-velocity fronts: Left: $v=1220$ m/s, elevation=81°, $g=30$ mm/km. Right: $v=1245$ m/s, elevation=76°, $g=25$ mm/km; Bottom: geographical relationships. Note that the actual front may be smaller than indicated in the plots.

For the proposed threat model for Germany, cf. Fig 11 and Fig 12, we have computed the vertical position error caused by anomalous ionosphere at an aircraft for distances of 6 km and 23 NM from the GGF. Since the vertical error depends on the GPS constellation, on details of the approach and on the used subset of visible GPS satellites, we show a histogram of errors. It contains the errors for all subsets of satellites and all combinations of impacted satellites for all epochs within 24 hours.

Performing simulations similar to refs. [4] and [5], we obtain for each epoch the so-called maximum ionosphere error in vertical (MIEV) defined as

$$MIEV = |\varepsilon_1 \cdot s_{vert,1} + \varepsilon_2 \cdot s_{vert,2}|,$$

where $s_{vert,1}$ and $s_{vert,2}$ are the projections to the vertical errors of satellite 1 and 2 and ε_1 and ε_2 are the worst-case link errors obtained from the simulation using the threat model. In Fig 17 the MIEV histograms are shown for two different aircraft to GGF distances. For a separation of GGF and aircraft of 6 km, the maximal MIEV is less than 20 m. This is less than the $VAL_{H2,I}$ of 28.8 m at decision height [8], indicating that here the use of geometry-screening may not be necessary, while in CONUS the MIEV exceeds clearly $VAL_{H2,I}$.

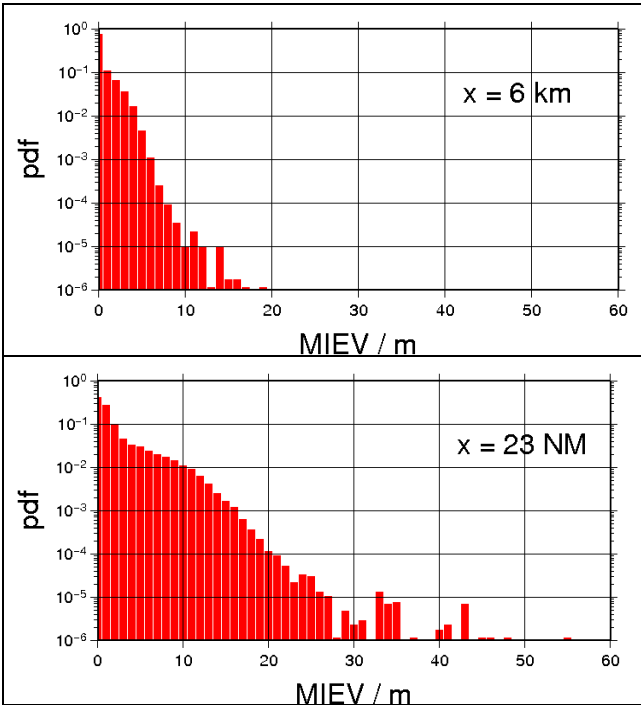


Fig 17: MIEV-Histogram for the threat model for Germany for aircraft-ground station distances of 6 km (top) and 23 NM (bottom), respectively. We used the GPS-constellation of Jan 2, 2007. The location for which the MIEV-values were calculated is Bremen ($X=3787999.8990$ m, $Y=573746.4640$ m, $Z=5082265.995$).

CONCLUSIONS AND OUTLOOK

For the region “Germany”, we have performed a data screening in order to identify periods with anomalous ionosphere activity using all publicly available RINEX data from the 11-year period 1998-2008. As a result of the data screening, 16 time periods with anomalous ionosphere activity were identified.

Then, for each of these time periods, additional data from the German geodetic network SAPOS was analyzed in order to determine the ionosphere threat space for Germany. 26 ionosphere fronts were analyzed w.r.t. threat model parameters. As a result, a threat space valid for the mid Europe especially Germany was derived.

The maximal gradients found over Germany are much smaller than the gradients found in CONUS. However, we have found events velocities exceeding 800 m/s with slopes less than 50 mm/km. While these high-velocity events are not relevant for CAT-I systems, they may be an issue for the future CAT-III /GAST-D systems.

In addition to the extreme ionosphere behavior, which is captured by the anomalous ionosphere threat model, we have also determined the nominal ionospheric gradients in the considered region using calibrated vertical ionospheric delays from periods of quiet to moderate ionospheric activity.

The results act as an essential input for further parameterization and certification of GBAS systems in Europe.

ACKNOWLEDGEMENTS

We thank IGS, EUREF, GREF and SAPOS for data provision.

REFERENCES

- [1] Christoph Mayer, Boubeker Belabbas, Winfried Dunkel, “Ionospheric Threat Model Assessment”, ICAO NSP Meeting, 2009-03-17 - 2009-03-20, EUROCONTROL Experimental Centre, Bretigny (France); <http://elib-v3.dlr.de/58489/>
- [2] Mayer, Christoph und Jakowski, Norbert und Borries, Claudia und Pannowitzsch, Thomas und Belabbas, Boubeker, “Extreme ionospheric conditions over Europe observed during the last solar cycle” 4th ESA Workshop on Satellite Navigation User Equipment Technologies, Dec 10 – Dec 12 2008, ESTEC, Noordwijk (The Netherlands); <http://elib-v3.dlr.de/58486/>
- [3] Pullen, Sam, Park, Youngshin, and Enge, Per *The Impact and Mitigation of Ionosphere Anomalies on Ground-Based Augmentation of GNSS*, Presented May 2008 at the 12th International Ionospheric Effects Symposium, Alexandria, VA; <http://waas.stanford.edu/~www/papers/gps/PDF/PullenIES08.pdf>
- [4] Ramakrishnan, Shankar, Lee, Jiyun, Pullen, Sam, and Enge, Per, *Targeted Ephemeris Decorrelation Parameter Inflation for Improved LAAS Availability during Severe Ionosphere Anomalies* Presented January 2008 at the ION Institute of Navigation National Technical Meeting, San Diego, CA; <http://waas.stanford.edu/~www/papers/gps/PDF/RamakrishnanIONNTM08.pdf>
- [5] Lee, Jiyun, Luo, M. Pullen, S., Park, Y. S., Enge, P., and Brenner, M. *Position-Domain Geometry Screening to Maximize LAAS Availability in the Presence of Ionosphere Anomalies* Presented September 2006 at the ION Institute of Navigation Global Navigation Satellite Systems Conference, Fort Worth, TX; <http://waas.stanford.edu/~www/papers/gps/PDF/LeeIONGNSS06.pdf>
- [6] Jakowski, N., *TEC Monitoring by Using Satellite Positioning Systems*, in Modern Ionospheric Science, (Eds. H. Kohl, R. Rster, K. Schlegel), EGS, Katlenburg-Lindau, ProduServ GmbH Verlagsservice, Berlin, pp 371-390, 1996
- [7] <http://swdcwww.kugi.kyoto-u.ac.jp/dstdir/>
http://www.ngdc.noaa.gov/stp/GEOMAG/kp_ap.html

- [8] Curtis A. Shively and Rick Niles, *Safety Concepts for Mitigation of Ionospheric Anomaly Errors in GBAS*, Proceedings of the 2008 National Technical Meeting of the Institute of Navigation January 28 - 30, 2008, San Diego, CA